J Sol-Gel Sci Technol (2017) 83:596–608
DOI 10.1007/s10971-017-4460-6

ORIGINAL PAPER: NANO-STRUCTURED MATERIALS (PARTICLES, FIBERS, COLLOIDS, COMPOSITES, ETC.)

Influence of sol–gel derived strontium–cerium co-substitution in fluorohydroxyapatite and its in-vitro bioactivity

Vijayalakshmi Sanyal[1] · **C. Ramachandra Raja**[1]

Received: 16 June 2016 / Accepted: 26 June 2017 / Published online: 17 July 2017

Abstract The present study is to investigate the influence of Sr^{2+} and Ce^{3+} ions in the structure of fluorohydroxyapatite (FHA) ($Ca_{10}(PO_4)_6F_{0.5}(OH)_{1.5}$), a partial substitution of fluorine ion in hydroxyapatite. Co-substitution of Sr^{2+} and Ce^{3+} ions improves the osteoblast cell response, an important factor which stimulates the bone formation surrounding the implant material. Sol–gel derived fluorohydroxyapatite samples were co-substituted with Sr^{2+} and Ce^{3+} ions [xSr/yCe-FHA, where $x = 5$–40 mol% of Sr^{2+} and $y = 5$–20 mol% of Ce^{3+}]. The intensity variation and shift of Fourier transform infrared bands observed after the co-substitution of Sr^{2+} and Ce^{3+} ions confirmed the doping. The X-ray diffraction shows the decrease in crystallite size with Ce^{3+} concentration and aids in forming beta-tri calcium phosphate and cerium-oxide (CeO) phases. Co-substitution of Sr^{2+} and Ce^{3+} increases the microhardness and fracture toughness, while micro structural analysis reveals the decrease in grain size. In-vitro bioactivity studies were conducted on samples using human osteosarcoma MG63 cells to investigate the osteoblast cell response. Co-substitution of cations in fluorohydroxyapatite by sol–gel method influenced the structure, phase formation, mechanical property, and grain size. These factors due to addition of Sr^{2+} and Ce^{3+} ions in fluorohydroxyapatite are attributed to the improvement of cell viability and alkaline phosphatase (ALP) activity.

Graphical abstract

- XRD patterns confirm co-substitution of strontium and cerium ions in fluorohydroxyapatite.
- Co-substitution of Sr^{2+} and Ce^{3+} ions in FHA enhances in-vitro bioactivity.

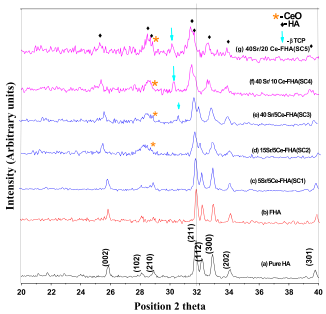

XRD patterns of HA, FHA and Sr/Ce doped FHA samples.

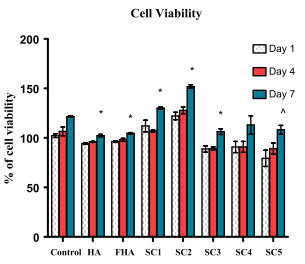

Comparison of cell viability of Sr/Ce-FHAwitl control

Keywords Sol–gel process · Fluorohydroxyapatite · X-ray studies · Mechanical properties · Osteoblast · Alkaline phosphatase activity

1 Introduction

Bone, the connective tissue is associated with a number of health issues which needs treatment such as repair or replacement. The hard tissue is resorbed and regenerated continuously by a balance between osteoclastic (bone resorption) and osteoblastic (bone formation) activity. This remodeling process heals minor bone defect while additional stimulation is required for bone formation in the case of implantation or

✉ C. Ramachandra Raja
crrajaphy@gmail.com
crraja_phy@yahoo.com

[1] Department of Physics, Government Arts College (Autonomous), Kumbakonam, Tamilnadu 612002, India

bone replacement. Hydroxyapatite (HA-$Ca_{10}(PO_4)_6(OH)_2$) is the bioceramic material of wide interest for application in orthopedic implants and has received a focus over three decades. The biocompatible apatite closely resembles the mineral phase of human bone and teeth but lacks mechanical strength and bioactivity [1–3].

Natural apatite in bone along with calcium, phosphate, and hydroxyl group has trace elements such as CO_3^{2-}, Na^+, K^+, Mg^{2+}, Sr^{2+}, Cl^-, F^-, Zn^{2+}, Cr^{3+}, Co^{2+}, Mn^{2+}, and Si^{4+} [4]. Substitution of metal ions in synthetic HA, replacing the Ca^{2+}, PO_4^{3-}, and OH^- ions modifies the solubility, mechanical properties and bone bonding ability. As an essential trace element of bone which improves the mechanical properties, a lot of interest has been directed towards the fluorohydroxyapatite (FHA-$Ca_{10}(PO_4)_6(OH)_{2-2x}F_{2x}$), a partial substitution of fluorine ion in HA [4–7]. Lower concentration of F^- ions incorporated in HA induces bioactivity while higher fluoride level results in an undesirable effect causing osteomalacia. It is also reported that with the addition of F^- the solubility decreases [5–9]. Many researchers have reported that the F^- ions of range x being 0.4–1.0, improves the mechanical properties, chemical and thermal stability [10–12]. Improvements of osteogenic potential in FHA coatings are achieved with $x = 0.8$–1.1 fluorine concentration [13]. Qu and Wei et al. [14] observed higher amount of protein and proliferation rate for 0.3–0.567 F^-/mol concentration.

Sr^{2+} in HA has been reported to enhance the osteoblast activity and inhibit resorption [15–21]. Strontium containing calcium phosphate bone cement is said to increase the mechanical strength and is used in the treatment of osteoporosis. Strontium in a stable form is non-toxic and even administered in the larger doses in the human body which always favors the mechanical and biological properties [23–29]. In biomedical field, the post-surgical infection is a frequent problem confronted which ultimately leads to the removal of the implants. The adhesion of bacteria on the surface of the implant develops infection and forms a biofilm which affect the tissue-implant integration. The long term in-vivo performance of any implants could be affected for similar reasons. Cerium, the lanthanide element is an antibacterial agent and when doped in HA exhibits antibacterial property against micro-organisms [30–32]. The trivalent Ce^{3+} also change the surface property which enhances the structural stability, bioactivity while altering the dissolution rate [33]. Studies have been reported on the improved bioactivity HA doped with trivalent and divalent cations. Researchers have suggested that the osteoblast activity is enhanced in the case of trivalent doped HA. The increase in valence of doped cations improve the biocompatibility of the HA ceramics [18–20, 31–34].

The clinical success of an implant depends upon both stable implant-tissue osteointegration and its mechanical properties. For remodification of bone, the most important factor is that the implant should support and improve bone cell formation. Despite good osseointegration, the implant should also have improved mechanical properties. Several studies have been reported on the ionic substitution and its enhancement of properties [4]. Recent focus on co-substitution of metal ions in hydroxyapatite improves the overall performance of the materials [10, 27, 28, 31, 32]. The surface of the implant should give rise to osteoconduction by cell viability and differentiation towards bone cell formation which reconstructs the bone. Before fixation of the implant in the human body it is most essential for an in-vitro cell study which includes cell viability and differentiation (alkaline phosphatase (ALP) activity) which gives the entire information of the behavior of the implant. The MG 63 Human osteosarcoma osteoblast cells are used to analyze the bone cell formation and remodeling features. In the present study strontium–cerium ions are co-substituted in FHA and investigated for the physico-chemical properties and cell parameters, which have significantly contributed to the improvement of both mechanical and biological performances.

Sol–gel technique has been used to prepare nanomaterials, as the partially hydrolyzed gel forms a network which facilitates the structure evolution, reduces particle size, and lowers the processing temperature with excellent chemical homogeneity [35–38]. Researchers have reported about substitution of metal ions in hydroxyapatite which alters either mechanical or biological properties [5–7, 11–27, 33, 34]. This technical paper is an attempt to investigate the synergetic effect of both mechanical properties and in-vitro bioactivity of Sr/Ce co-substituted in FHA. The present work aims to investigate the influence of Sr^{2+} and Ce^{3+} cation co-substitution in fluorohydroxyapatite using spectral, mechanical, and biological characterization techniques. Samples of pure HA, FHA, xSr / yCe-FHA ($x = 5$–40 mol% Sr^{2+} and $y = 5$–20 mol% Ce^{3+}) [$Ca_{10-x-y}Sr_xCe_y(PO_4)_6(OH)_{1.5}F_{0.5}$] with 25% of F^- are synthesized. The hardness and fracture toughness are measured for analyzing mechanical properties. As the part of bioactivity, the cell viability and ALP activity are evaluated and analyzed for improvement in osteoblast performance.

2 Materials and methods

2.1 Fabrication

2.1.1 Pure HA

Hydroxyapatite [$Ca_{10}(PO_4)_6(OH)_2$] is prepared using analytical grade chemicals calcium nitrate tetrahydrate [$Ca(NO_3)_2.4H_2O$] and orthophosphoric acid (H_3PO_4) as

precursors by sol–gel method. A sol is prepared by drop wise addition of 1.0 M calcium nitrate tetrahydrate solution with 0.25 M orthophosphoric acid (H_3PO_4) solution so as Ca/P molar ratio is 1.67. De-ionised water is used as the solvent for all the solution preparation. In order to obtain the pH as 10, ammonia solution is added to sol. The sol is aged after an hour of vigorous stirring and is kept at ambient temperature for 24 h. The sol when maintained in a temperature of 65 °C in a constant temperature bath transforms it into a white gel of uniform consistency. The dried gel is repeatedly washed with deionsed water for the removal of nitrates. The sample is further heated to 200 °C and manually ground using mortar and pestle to obtain powder HA.

2.1.2 Strontium–cerium fluorohydroxyapatites (xSr/yCe-FHA)

The precursors strontium nitrate [$Sr(NO_3)_2$], cerrous (III) nitrate[$Ce(NO_3)_3$] hexahydrate and ammonium fluoride [NH_4F] were used for doping Sr, Ce, and F ions in HA. For all FHA samples the concentration of fluorine is kept as 25 mol%. The above said procedure is followed for the preparation of FHA and Sr/Ce-doped FHA of various concentrations [xSr/5Ce-FHA ($x = 5$, 15, 40 mol% Sr^{2+}) and 40Sr/yCe-FHA ($y = 5$, 10, 20 mol% Ce^{3+})]. In all cases (Ca + Sr + Ce)/P molar ratio is maintained as 1.67.

2.2 Sample preparation

To analyze the structure and morphology, the synthesized powders were calcined at 800 °C for 1 h. To study the osteoblast response of the synthesized material, the prepared powder samples were uniaxially cold pressed at 100 MPa into disks of 16 mm diameter, 1 mm thickness. These disks were sintered at 1200 °C for 2 h at the rate 10°/min and furnace cooled to room temperature. The Sr/Ce ions incorporated in FHA disks were subjected to biological studies such as cell viability and ALP activity.

2.3 Characterizations

2.3.1 Structural studies

The phase composition of the pure HA, FHA, and Sr/Ce-FHA composites were determined by XPERT PRO Diffractometer with CuKα radiation (40 mA, 40 kV). The scan range for 2θ was from 10° to 70°at a scan step time 0.05 s. The HA phase peaks are identified and indexed with standard data compiled by the JCPDS 09–432 (ICSD #087724). The phase composition, crystallite size and crystallinity of xSr/yCe-FHA (with different concentrations $x = 5$–40 mol% and $y = 5$–20 mol%) nanoparticles were determined for the calcined powder. As the (002) Miller plane perpendicular to c-axis, is sharper and isolated from other HA peaks it is chosen to calculate the crystallite size and crystallinity using Eqs. (1) and (2), respectively [31]

$$D_{(002)} = \frac{K\lambda}{\beta_{1/2}\mathrm{COS}\theta} \tag{1}$$

where $D_{(002)}$ is the crystallite size, λ is the wavelength of CuKα radiation (λ = 1.542 Å), $\beta_{1/2}$ is FWHM for the diffraction peak under consideration (in radians), θ is the diffraction angle and K is the broadening constant.

$$X_c = \left(\frac{0.24}{\beta_{(002)}}\right)^3 \tag{2}$$

where X_c is the degree of crystallinity and $\beta_{(002)}$ is the FWHM of (002) plane.

The lattice parameters such as "a" and "c" of all powders at different concentrations were calculated by using the Eqs. (3) and (4) respectively [7];

$$a = d \times \sqrt{\tfrac{4}{3} \times (h^2 + hk + k^2)} \quad \text{For } (hk0) \text{ planes} \tag{3}$$

$$c = l \times d \quad \text{For } (00l) \text{ planes} \tag{4}$$

where d is the distance between the planes and (hkl) are Miller planes.

The presence of the bands in Fourier transform infrared (FTIR) spectra confirmed the substitution of ions in HA. The KBr along with the synthesized samples were cold pressed to pellets in the weight ratio of 1:100. These pellets were subjected to Perkin Elmer spectrophotometer in the frequency range 4000–400 cm^{-1} and analyzed for functional groups.

2.4 Mechanical studies

The microstructures were characterized for morphology and grain size by field effect scanning electron microscope FESEM-EDAX (FESEM- Make JEOL, Model-JSM-6701F).

The micro-hardness of the samples was determined by a Vickers micro-hardness tester. For the calculation, the following formula was used [39],

$$H_v = 0.001854\frac{P}{d^2} \tag{5}$$

H_v is the Vickers Hardness (GPa); P is the applied load (N); d is the diagonal indent length (mm).

Fracture toughness of the samples was determined according to the length of the cracks "C" generated by the indentations applied during the micro-hardness test.

The Evans and Charles equation used to calculate the fracture toughness [41],

when C/a ratio is greater than 3,

$$K0em_{1c} = 0.0824\frac{P}{C^{1.5}} \quad (6a)$$

If C/a ratio is less than 3 then,

$$K_{1c} = 0.035\left(\frac{H^{0.6}E^{0.4}}{\phi^{0.6}}\right)\left(\frac{a}{(C-a)^{0.5}}\right) \quad (6b)$$

K_{1c} is the fracture toughness (MPa$\sqrt{m}$); P is the applied load (N); C is the crack length (m); a is the half length of diagonal (m); E is the Young's modulus of the material N/m^2; ϕ is the coefficient related to the material constraint and the value is 3.

Brittleness index, the combination of hardness and fracture toughness characterizes the deformation and fracture phenomenon of the solids from metals to ceramics. The brittle index is calculated as [40],

$$Brittleness\ Index = \frac{H_v}{K_{1c}} \quad (7)$$

2.5 Cell study

The antitumor assay was performed on osteoblastic cell lines MG-63 (Human Osteosarcoma cells) obtained from National Center for Cell Science (NCCS), Pune, India. The prepared disks of dimensions 16×1 mm were sterilized in the autoclave at 121 °C for 1 to 4 h before being cultured in 96-well plates to observe cell morphology, cell viability-cytotoxicity and ALP activity. The assays were performed in triplicates for each of the samples.

2.5.1 Cell viability

The MTT (3-(4,5-dimethylthiazol-2-yl)-2,5-diphenyltetrazolium bromide) tetrazolium (Himedia) reduction assay used for the analysis of cell viability. Cell culture was conducted in 96-well plate at 37 °C in a humidified 5% CO_2 atmosphere in a standard culture medium containing Dulbecco's Minimum Eagle's medium (DMEM), $pH = 7.4$ to 5 mg/ml supplemented with 10% bovine serum and 1% penicillin-G, streptomycin, amphotericin B.Cells were seeded on the sterilized pellets in the DMEM medium at a density of 1 x 10^4 cells/well and cultured up to 7 days. At each period (1, 4, and 7 days) the samples were taken out and removed to a new 24-well tissue cultured plates. The MTT substrate is prepared in a physiologically balanced solution, added to cells in culture, usually at a final concentration of 0.2–0.5 mg/ml, and incubated for 1 to 4 h. The formazan was solubilized by acidified 10% (vol/vol) of isopropanol and DMSO, 40% (vol/vol) of dimethylformamide, 2% (wt/vol) of SDS, and 2% of (vol/ vol) combinations of detergent and organic solvent [41]. The quantity of formazan (presumably directly proportional to the number of viable cells) is measured by recording changes in absorbance at 570 nm using a microplate reading spectrophotometer (Elx808 absorbance reader). Equation (8) is utilized to calculate the percentage of cell viability by comparing the effect of extract on treated cells to the control. The cell line MG 63 in DMEM without the samples (untreated) is the control. The untreated (control) after the first day is compared with the treated first day. Similarly the comparisons between untreated and treated are done for 4th and 7th day [41].

$$\%\ of\ cell\ viability = \frac{Treated\ cells\ group}{Untreated\ cell\ group(control)} \times 100 \quad (8)$$

2.5.2 Differentiation assay (ALP activity)

Intracellular ALP activity is analyzed for 14 days (1, 4, 7, and 14 day's interval) to evaluate the functionality of the cultured cells on Sr/Ce-doped FHA disks. In the colorimetric assay, using p-nitrophenyl phosphate as substrate, the ALP was measured for the cultured supernatants. The released p-nitrophenol was measured spectrophotometrically at 405 nm absorbance; presumably the released p-nitrophenol is proportional to the ALP activity. The 24-well plates were used to seed the MG-63 cells and treat the cultures with the prepared sample disks. Following the incubation period the cell free supernatants were collected for ALP assay. The procedures were triplicated and all the obtained results were compared against control and pure HA.

2.5.3 Statistical analysis

All data were expressed as mean standard deviation($n = 3$) and statistical analysis were carried out on cellular tests using one-way analysis of variance followed by *t*-test (or) Turkey's HSD using SPSS program (version 11.5). Differences were considered statistically significant at $p \leq 0.05$.

3 Results and discussion

3.1 Structure and morphology studies

XRD patterns of the calcined powder of pure HA, FHA, and Sr/Ce-doped FHA are depicted in Fig. 1a–g. The lattice parameters "a" and "c", crystallite size and crystallinity of

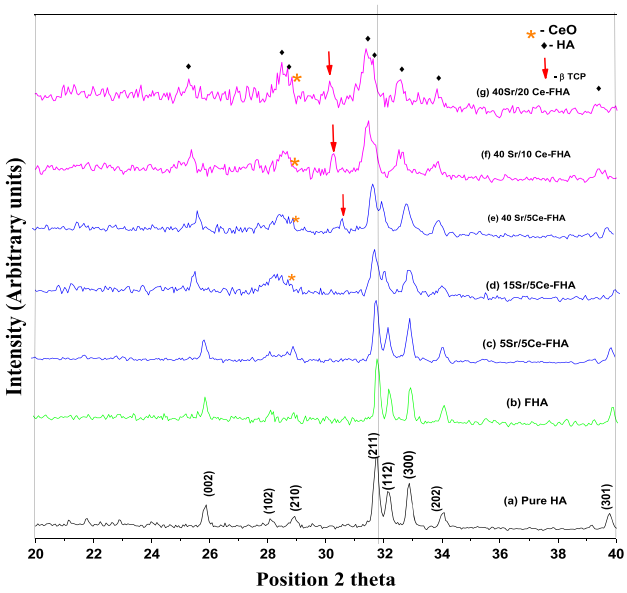

Fig. 1 XRD patterns of HA, FHA, and Sr/Ce-doped FHA samples. *HA* hydroxyapatite, *β-TCP* beta tricalcium phosphate, *CeO* cerium oxide

the pure and doped apatite samples are tabulated in Table 1. The peaks identified for pure HA (002), (210), (211), (112), (300), (202), and (310) confirmed the apatite formation. The crystallite size and crystallinity was calculated as 47.9 nm and 2.814. An increase in D_{002} and X_c is observed for the partial F^- ion substituted HA (FHA) sample. A shift is seen in the peaks of 2θ was observed and the sharper peaks of FHA correspond to the increase in X_c. The OH^- groups are oriented randomly due to a lesser affinity between the smaller ion H^+ and O^{2-} ions and it confers a certain degree of disorder [12]. In the FHA sample an affinity between F^-ions and O^{2-} ions are greater than the former and results in a well-ordered apatite structure and crystallinity increases. The absence of CaO and β-TCP secondary phases confirms the phase purity of the formed HA and FHA.

The Sr^{2+} ion (ionic radius—0.118 nm) and Ce^{3+} ion (ionic radius—0.101 nm) are co-substituted in the FHA samples to replace Ca^{2+}(ionic radius—0.100 nm) ion. The ionic substitution influences the lattice symmetry and structural characteristics resulting in the shift of peak intensity towards the lower value of 2θ (Fig. 1). In the case of higher substitution of Sr^{2+} (40 mol%) along with Ce^{3+} influences the lattice symmetry and favors the formation of beta-TCP phase. At lower concentrations of Sr^{2+} in samples 5Sr/5Ce-FHA and15Sr/5Ce-FHA, the formation of secondary phase such as beta-TCP is not distinguishable. The co-substitution of Ce^{3+} and Sr^{2+} to replace Ca^{2+} creates a charge imbalance and is compensated by Ca^{2+} vacancies which favor the formation of beta-TCP phase [34]. As Ce^{3+} concentration increases, the peak intensity is shifted towards the lower 2θ value and this not only favors beta-TCP phase but also gives rise to an additional CeO phase. The presence of the peaks related to the beta-TCP and CeO confirms the phase formation (Fig. 1). It is reported that the solubility of TCP is more when compared with HA [42].

The 5 mol% each of Sr^{2+} and Ce^{3+} ion in FHA has decreased the crystallite size and crystallinity. As the ionic radius of Sr^{2+} is greater than Ce^{3+} the increase in Sr^{2+} concentration from 5 to 40 mol% has shown an increase in crystallite size and lattice parameters. The electro negativity of Ca^{2+} (0.99) is close to Sr^{2+} (0.95) and Ce^{3+} (1.04) giving rise a stable apatite structure with the doping concentration. Greater the electric charge of ions, greater would be the lattice energy influencing the stability of the crystal structure [28, 33]. The crystallite size decreases upon increasing the Ce^{3+} content. Ce^{3+} has more electric charge than Ca^{2+} which is replaced. A stability is achieved on doping Ce^{3+} ions and during nucleation more nuclei is formed which leads to decrease in crystal size. Also the ionic radius of Sr^{2+} and Ce^{3+} are slightly greater than Ca^{2+} which blocks the crystal growth and reduces the crystallite size. The drastic decrease in crystallinity on the Sr^{2+} content was observed and it agrees with the literature. Along with peak broadening the decrease in intensity of (300) peak is also observed for higher concentration of dopants (40% Sr^{2+} and 10, 20 % Ce^{3+}) leading to decrease in crystallinity [43].

The ten of calcium atoms of HA ($Ca_{10}(PO_4)_6(OH)_2$) are arranged in such a way, that four are at Ca(I) site aligned in column surrounded by nine oxygen atoms. The other six are arranged in equilateral triangle at Ca(II) site each surrounded by seven oxygen atoms. The dopant metal ions have the tendency of occupying both Ca(I) and Ca(II) sites. Recent study have revealed the preferential occupancy of Ca(I) site for lower concentration of dopant ions. As the concentration exceeds 10 mol% the Ca(II) site is also occupied. The occupancy of Ca(I) and Ca(II) site leads to increase in lattice parameters “a” and “c” which is in agreement with literature [44]. Moreover Ce^{3+} doping influences the growth along c-axis with increase in “c” parameter and is evident from the Table 1 [33]. This preferably suggests that occupancy of co-substitution of Sr^{2+} and Ce^{3+} ions favors Ca (II) site for higher concentrations. A structural strain is evident from the peak broadening caused by the incorporation of larger ions in FHA and further the shift of 2θ confirms the efficient incorporation of Sr^{2+} and Ce^{3+} ions in the FHA structure.

The FESEM micrographs reveal the morphology and composition of the entire samples with EDAX analysis as shown in Fig. 2a–g and Table 2. It is evident from the morphology study that the obtained particles by sol-gel method are nanoparticles. Spherical shaped particles were observed for HA, FHA and their size ranged from 100 to

Table 1 Lattice parameters, crystallite size and crystallinity

Sample name	Lattice parameters in Å		Volume in Å^3	Difference in lattice parameters and volume			Crystallite size D_{002} in nm	Crystallinity X_c
	a = b	c		Δa in Å	Δc in Å	ΔV in Å^3		
Pure HA -HA	9.436	6.887	531.1	—	—	—	47.9	2.814
FHA -FHA	9.444	6.892	532.7	0.008	0.005	1.60	60.5	4.342
5Sr/5Ce-FHA -SC1	9.560	6.910	546.9	0.124	0.023	15.80	55.3	3.573
15Sr/5Ce-FHA -SC2	9.562	6.928	548.5	0.126	0.041	17.4	57.3	2.813
40Sr/5Ce-FHA -SC3	9.573	7.011	556.3	0.137	0.124	25.2	65.4	1.813
40Sr/10Ce-FHA-SC4	9.541	7.052	555.9	0.105	0.165	24.8	13.1	0.067
40Sr/20Ce-FHA-SC5	9.472	7.063	548.7	0.036	0.176	17.6	20.7	0.226

110 nm, 90 to 120 nm respectively. As the concentration of Sr^{2+} increased from 5 to 40 mol% (xSr/5Ce-FHA, $x =$ 5–40 mol% Sr) the spherical agglomerated particles increased in size to 100–150 nm (Fig. 2). The increase in concentration of Ce^{3+} (40Sr/yCe-FHA, $y = 10$, 20 mol% Ce), has resulted in elongated particles, as cerium ions promote the growth of the crystallites along c-axis. The obtained XRD pattern and the FESEM studies confirm the above result [33]. The length and breadth of the particle are nearly 100 and 20 nm respectively which resembles a short rod as shown in Fig. 2.

3.2 FT-IR spectral studies

The FT-IR spectrum revealed major phosphate and hydroxyl peaks related to HA and is shown in Fig. 3a. The additional features unique to FHA and Sr/Ce-doped FHA are also observed in the studies (Fig. 3b–g).

The phosphate bands (PO_4^{3-}) exhibited by pure HA are bending vibration (ν_2)O–P–O at 472 cm^{-1}, bending vibration (ν_4) O–P–O at 568 and 602 cm^{-1}, asymmetric stretching (ν_1) at 1040 and 1092 cm^{-1} indicating the formation of pure HA phase. The peak 633 cm^{-1} is attributed to OH^- liberation and 1614 cm^{-1} represents bending vibration of water. The broad and an extended band from 2900 to 3600 cm^{-1} represents the stretching modes of hydrogen bonded H_2O molecules [45].

The presence of the peak around 720–740 cm^{-1} is attributed for the incorporation of fluoride ions in HA lattice [46]. In Fig. 3b the peak at 718 cm^{-1} is the evidence for addition of F^- ions into HA structure. The decrease in intensity of hydroxyl group at 633 cm^{-1} and the presence of the band at 3538 cm^{-1} confirms the formation of OH–F bond [10].

On co-substituting Sr/Ce in FHA, and when the concentration of Sr^{2+} ion increases from 5 to 40% a shift of phosphate peaks were observed. The peak at 571 cm^{-1} shifts towards lower frequency 568 cm^{-1} and similarly the peak at 604 shifts to 600 cm^{-1}. These shifts are attributed to the effective incorporation of Sr^{2+} ions. The substituted cation has increased dimensions which results in anion-anion separation [44, 47–49]. The shifting of 633 cm^{-1} towards lower frequency 569 cm^{-1} on increasing the cation concentration is ascribed to the incorporation of larger ionic radius (Sr^{2+} and Ce^{3+} replacing Ca^{2+}) in the lattice [50]. A similar shift of OH^- peaks and intensity decrease are reported in case of divalent substitution in HA lattice [48]. The band at 3435 cm^{-1} is attributed to the stretching of metal—OH bond. As Sr^{2+} and Ce^{3+} ion of greater ionic radius are co-substituted a shift from 3435 cm^{-1} to 3429 cm^{-1} was observed. Structural stability of Sr/Ce-FHA samples is confirmed by the absence of broadening of phosphate bands [28].

3.3 Mechanical studies

Vickers microhardness (H_v), fracture toughness (K_{1c}) and brittleness index (B.I) of pure HA and Sr/Ce-FHA samples are calculated using Eqs. 5, 6a, 6b, and 7 and are tabulated in Table 2. The corresponding microstructures are shown by the FESEM micrographs in Fig. 4. The value of Pure HA was found to be 4.15 ± 0.21 GPa. Addition of F^- has slightly increased the microhardness to 4.68 ± 0.30 GPa. Fracture toughness of pure HA and FHA was found to be 0.66 MPa m$^{1/2}$ and 0.94 MPa m$^{1/2}$ respectively. The pure HA shows small, loosely packed grains with pores of size 1–1.5 μm. Similar microhardness and fracture toughness results were reported for pure HA [12, 40]. The microstructure of F^- addition has shown the grain size of range 0.7–1.2 μm. The affinity between metal ion and F^-/OH^- has increased the compactness with some pores and thus increases H_v and K_{1c} value [10].

The addition of Sr content from 5 to 40% increases H_v and K_{1c} to 5.85 ± 0.12 GPa and 1.36 ± 0.05 MPa m$^{1/2}$ respectively and is shown in Table 3. The Sr/Ce dopant in FHA has decreased the grain size. The grain size of the

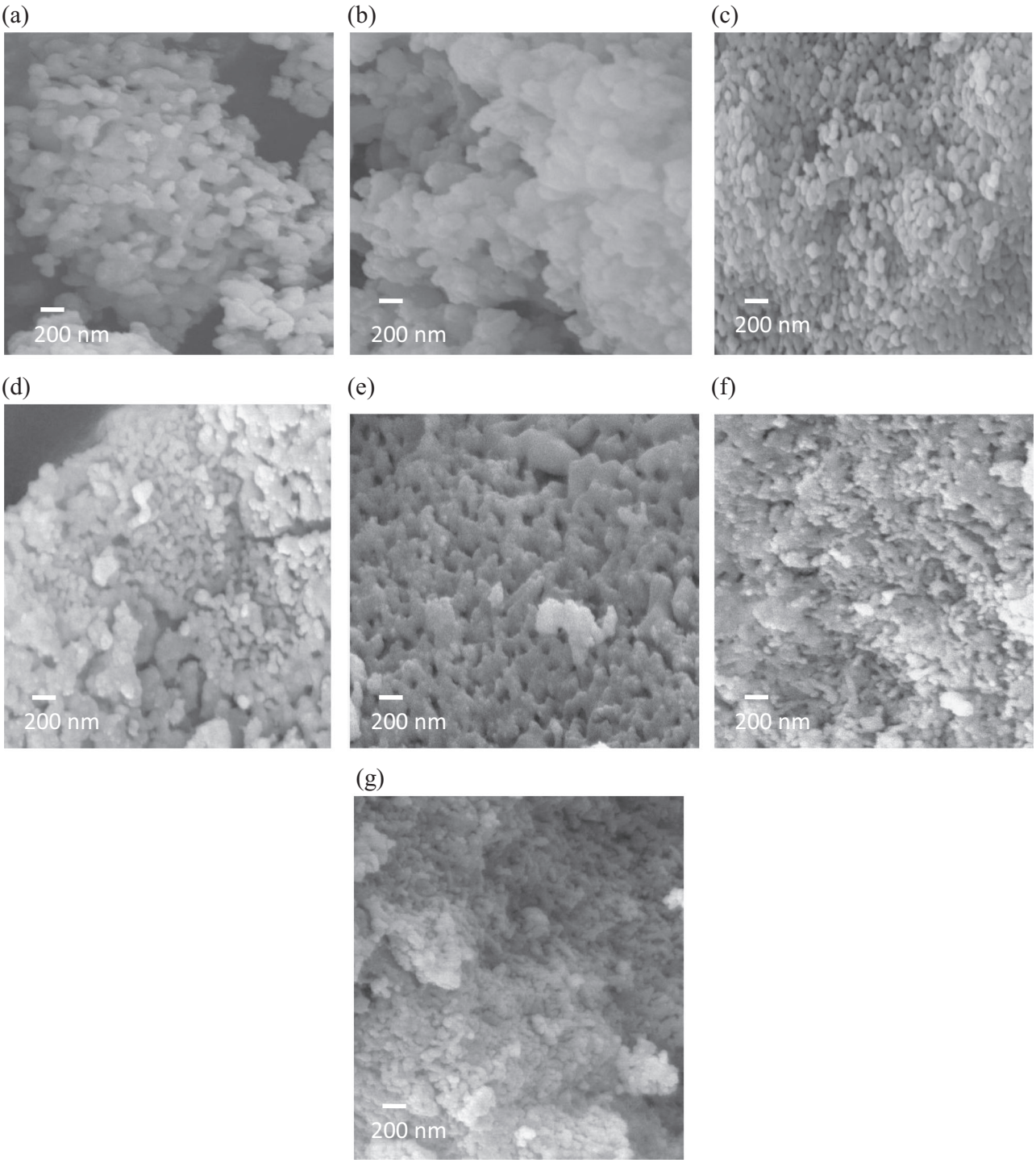

Fig. 2 **a–g** FESEM micrographs of HA, FHA, and Sr/Ce-doped FHA. **a** Pure HA, **b** FHA, **c** 5Sr/5Ce-FHA, **d** 15Sr/5Ce-FHA, **e** 40Sr/5Ce-FHA, **f** 40Sr/10Ce-FHA, **g** 40Sr/20Ce-FHA

samples15Sr/5Ce-FHA and 40Sr/5Ce-FHA decreases to 0.69 and 0.58 µm, respectively and their sintered density also increases which closes the pores in these samples. The grain size and morphology influences the H_v and K_{1c} value. Decrease of grain size has improved the H_v and K_{1c} value for better mechanical strength, as smaller grains do not favor crack propagation. The FESEM micrograph (Fig. 4d, e) shows compact grains without pores as well plate-like morphology on Sr/Ce co-substitution. The addition of Sr/Ce has favored the reduction of grain size. Along with coarse grains, fine grains of 0.16 µm are also seen which are due to the secondary phase's beta-TCP and CeO, while the XRD is

Table 2 EDAX- mole fraction of elements

Sample name	Mole fraction of elements				
	Ca	P	Sr	Ce	F
HA	0.977	0.532	–	–	–
FHA	0.970	0.571	–	–	–
5Sr/5Ce-FHA	0.894	0.595	0.032	0.053	0.048
15Sr/5Ce-FHA	0.760	0.487	0.171	0.055	0.045
40Sr/5Ce-FHA	0.440	0.424	0.295	0.052	0.048
40Sr/10Ce-FHA	0.430	0.411	0.286	0.183	0.049
40Sr/20Ce-FHA	0.406	0.411	0.289	0.212	0.048

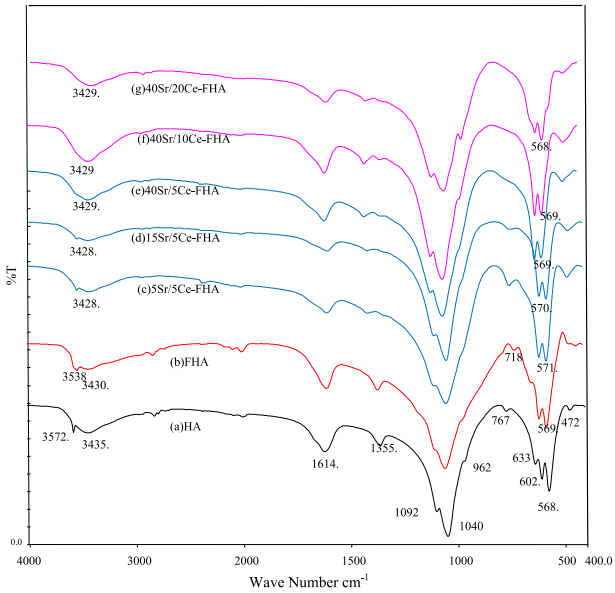

Fig. 3 a–g. FT-IR of the HA, FHA and doped FHA samples

also consistent with the phase formation. These fine grains increase with the increase of Ce content to 10 and 20% and are visible in the grain boundary in Fig. 4e–g. The fine CeO phases found in between the grains change the grain pattern giving rise to interconnected pores of size 1–1.2 µm. This decreases the mechanical strength of the material.

Hardness and fracture toughness are the parameters which characterizes the deformation and fracture phenomenon in ceramics. Brittle index (BI) is the ratio of hardness and fracture toughness which analyze the material for mechanical strength The decrease in BI favors the mechanical strength of the material [40]. The pure HA and FHA has the Brittleness Index as 6.30 ± 0.25 and $5.0 \pm 0.10\ \mu m^{-0.5}$ respectively while the co-substitution of Sr/Ce in FHA (40Sr/5Ce-FHA) has a lower BI as $4.30 \pm 0.07\ \mu m^{-0.5}$.

3.4 Cell viability

Figure 5a–h shows the cell viability (MTT assay) of MG-63 osteoblast cells with Sr/Ce in FHA for 7th day along with the positive control and HA. The optical density in microplate reader is recorded with 570 nm wavelength and is proportional to the number of cells formed.

The percentage of cell viability was calculated using the Eq. (8). Figure 6 shows the graphical representation of the cell viability for concentrations on 1st, 4th, and 7th days and is compared with positive control and HA.

Studies have reported that increase in the valence of the doped cations can improve the biocompatibility [10, 15–17, 26]. Webster et al has concluded trivalent doped apatite showed better cell adherence to the surfaces than divalent dopants [19]. The bone forming cells are also dependent on resorption of the HA, while literature has proved the formation of beta-TCP phase is proportional to resorption [15–17, 26, 42].

No significant differences were observed in cell morphology for all concentrations of Sr/Ce ions. It is evident from Fig. 6 that the cells grew favorably and has spread over the sample disks. The observed cells were flattened with their filapodium and lamellipodium suggesting improved cell viability due to co-substitution of Sr/Ce in FHA. Cell viability was found to increase with time in culture for variable doses of Sr^{2+} and Ce^{3+} in FHA. In all the tested samples no down regulation was observed which also confirms there is no cytotoxic effect (Fig. 6). The cell viability of HA and FHA also increased with time and recorded a positive regulation.

Co-substitution of Sr^{2+} and Ce^{3+} has exhibited the beta-TCP phase confirming the resorption which in turn influences the bone cell formation. As the Sr^{2+} content increased from 5 to 15 % an elevation in the cell viability was observed. Cell viability from day1 to 4 is sustained, while a greater proliferation occurs between 4 and 7th day resulting in an increased osteoblast formation which was also in agreement with literature [18]. The percentage of cell viability for 15Sr/5Ce-FHA (SC-2) was higher over all the other samples and a maximum cell density was observed for this sample. This may be attributed to controlled and continuous release of ions which has significantly improved the osteogenic cell response. The rapid release due to higher concentration of dopants decreases the osteoblastic activity [10, 16, 18, 19]. The presence of optimum concentration of Sr^{2+} with Ce^{3+} in SC-2, has favored the osteoblast.

The release of Sr^{2+} in the environment does not always provoke the osteoblasts, as higher concentration of dopants results in gradual decrease of osteoblast activity [13, 18]. It is evident that the concentration variation distorts the lattice and develops a secondary phase such as beta-TCP and cerium oxide phase. Collectively, higher concentration of

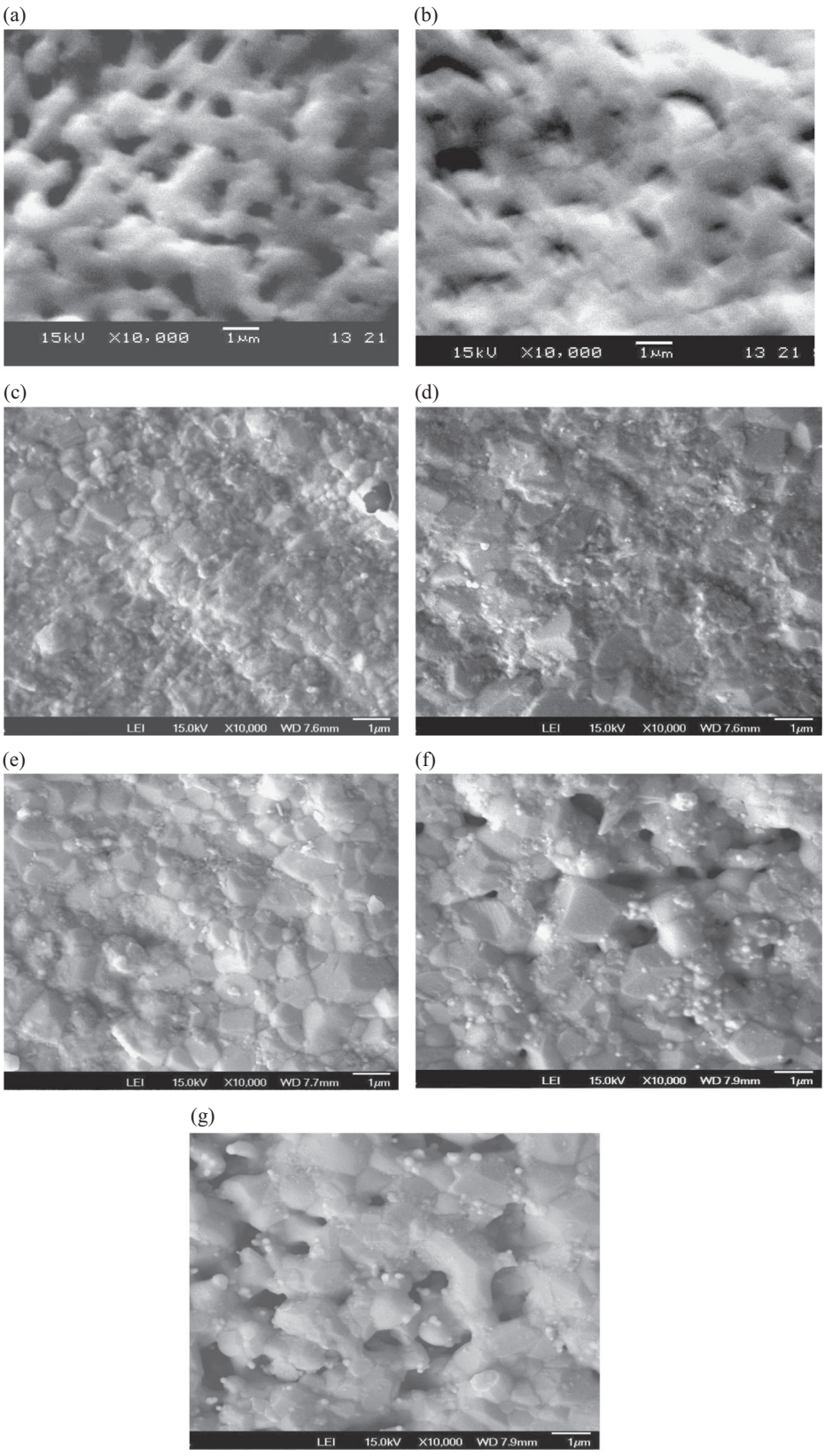

Fig. 4 **a–g** Microstructures of pure HA and Sr/Ce-FHA. **a** HA, **b** FHA, c 5Sr/5Ce-FHA-SC1, **d** 15Sr/5Ce-FHA-SC2, **e** 40Sr/5Ce-FHA-SC3, **f** 40Sr/10Ce-FHA- SC4, **g** 40Sr/20Ce-FHA-SC5

Sr^{2+} along with Ce^{3+} (SC3, SC4, and SC5) inhibits the cell proliferation when compared to control. The decrease in cell viability percentage for higher dopant concentration would be due to biodegradability developed by the beta-TCP and cerium oxide phase.

3.5 ALP activity

The early differentiation marker, ALP activity, is associated with calcification, enhancement of mineralization and enrichment of inorganic phosphate, one of the important components of mineral phase of the bone. The early differentiation marker, release of Sr^{2+} ion in the fluid, increases the ionic activity followed by induced fluorohydroxyapatite precipitation. The Sr^{2+} induces the cell metabolism resulting in the formation of protein matrix, the fibrous tissue and the precipitated fluorohydroxyapatite is embedded with it [18–20]. Many researchers have reported on ALP activity for SrHA [13–21]. Researchers have also reported that, the addition of Ce^{3+} into apatite has the antibacterial activity [32–34]. The present study suggests the improvement of ALP activity due to the co-substitution of Sr/Ce ions in FHA.

Figure 7 shows that the ALP activity of MG63 cells on Sr/Ce- FHA disks for 14 days and is compared with control and HA. All the samples till 7th day showed a positive regulation of ALP activity and they were consistent.

A moderate ALP activity was marked for HA and FHA. The ALP activity of 5Sr/5Ce-FHA (SC 1) sample showed no noticeable variation from 1st to 14th day. Webster [19] has reported, the divalent doped HA ceramics, experiences a greater osteoblast activity during later days compared to earlier days and a trivalent doped shows appreciable osteoblast activity only in early days. A significant change of ALP levels was exhibited by the sample 15Sr/5Ce-FHA (SC 2) which promotes cell differentiation. Though a moderate level of ALP was seen till 7th day, from 7 to 14th day, an excellent improvement in ALP activity was specifically recorded only for sample 15Sr/5Ce-FHA (SC 2), which agreed with the literature. Increased solubility of FHA samples may be due to the presence of beta-TCP phase and thereby the precipitation of inorganic phosphate has resulted with improved ALP activity [42]. Even though a positive regulation of ALP activity was observed for higher concentration of Ce^{3+} (40Sr/10Ce-FHA (SC4) and 40Sr/20Ce-FHA (SC5)), the activity for 14th day compared to samples 15Sr/5Ce-FHA and 40Sr/5Ce-FHA shows a down regulation. Higher concentration of Ce^{3+} (10–20%) would rapidly increase the solubility of Sr/Ce co-substituted FHA, which reduces the early differentiation.

The present study reveals the Sr^{2+} with Ce^{3+} co-substituted samples 15Sr/5Ce-FHA (SC2) and 40Sr/5Ce-FHA (SC3) have exhibited a prominent ALP activity and

Table 3 Vickers microhardness (H_v), fracture toughness (K_{1c}) and brittleness index

Sample name	Sintered density g/cm^3	Vickers microhardness (H_v) GPa	Fracture toughness (K_{1c}) MPa (m)$^{1/2}$	Brittleness index Hv/ K_{1c} μm$^{-1/2}$	Grain size	
					Coarse grains μm	Fine grains μm
Pure HA	2.91	4.15 ± 0.21	0.66 ± 0.06	6.30 ± 0.25	1.36 ± 0.24	–
FHA	3.05	4.68 ± 0.30	0.94 ± 0.08	5.00 ± 0.10	0.96 ± 0.17	–
5Sr/5Ce-FHA	3.09	4.86 ± 0.17	1.02 ± 0.10	4.97 ± 0.28	0.33 ± 0.12	–
15Sr/5Ce-FHA	3.15	5.75 ± 0.07	1.32 ± 0.12	4.38 ± 0.15	0.69 ± 0.21	0.16 ± 0.04
40Sr/5Ce-FHA	3.10	5.84 ± 0.12	1.36 ± 0.05	4.30 ± 0.07	0.58 ± 0.19	0.18 ± 0.06
40Sr/10Ce-FHA	2.76	5.25 ± 0.09	1.19 ± 0.15	4.50 ± 0.39	0.70 ± 0.14	0.16 ± 0.05
40Sr/20Ce-FHA	2.57	5.12 ± 0.21	1.15 ± 0.17	4.52 ± 0.38	1.20 ± 0.14	0.21 ± 0.09

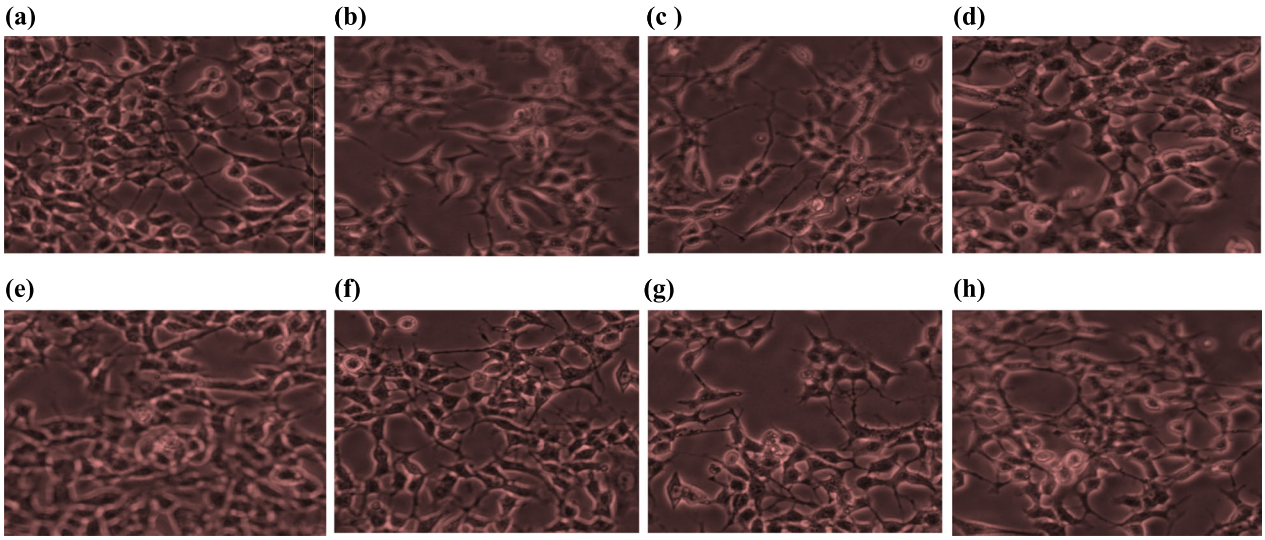

Fig. 5 **a–h** Cells cultured on the sample pellets shows the cell viability after 7days with control. **a** Control, **b** Pure HA, **c** FHA, **d** 5Sr/5Ce-FHA (SC1), **e** 15Sr/5Ce-FHA(SC2), **f** 40Sr/5Ce-FHA (SC3), **g** 40Sr/10Ce-FHA(SC4), **h** 40Sr/20Ce-FHA(SC5)

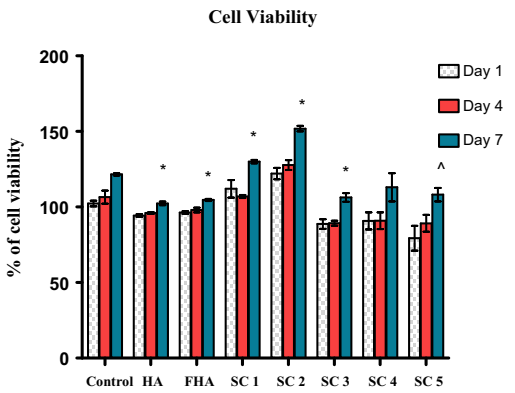

Fig. 6 Comparison of cell viability of Sr/Ce-FHA. Data = Mean ± SD; $n = 3$, $*p \leq 0.05$, $\wedge p < 0.1$ compared to control

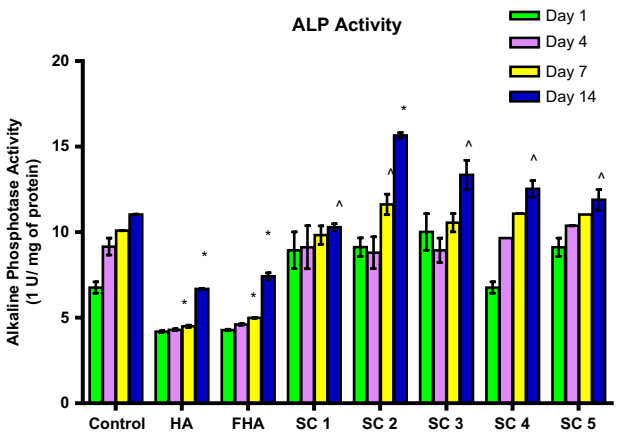

Fig. 7 The ALP activity of Pure HA and doped Sr/Ce-FHA. Data = Mean ± SD; $n = 3$, $*p \leq 0.05$, $\wedge p < 0.1$ compared to control

stimulates the cell differentiation. Thus, the ALP activity for the sample 15Sr/5Ce-FHA (SC2) follows the cell viability and highlights the biological performance.

4 Conclusion

- Sol–gel derived Sr^{2+} /Ce^{3+} co-substitution of FHA has resulted significant improvement in mechanical and biological properties.
- The XRD and FT-IR patterns confirm the co-substitution of Sr^{2+} and Ce^{3+} in the crystal structure.
- The samples 15Sr/5Ce-FHA and 40Sr/5Ce-FHA have higher hardness (H_v) value than HA and also the fracture toughness K_{1c} has increased to twice of HA.
- The samples subjected to analysis of biocompatibility, percentage of cell viability and ALP activity was found to exhibit an improved osteoblast cell response.
- Incorporation of Sr^{2+} and Ce^{3+} in FHA samples favored the formation beta-TCP phase which increases the solubility of FHA. This increase in solubility improves bioactivity by the release of ions and is confirmed by the ALP activity of the sample 15Sr/5Ce-FHA (SC2).
- Sr^{2+} with Ce^{3+} co-substituted FHA improves the osteoblast cell response. The samples 15Sr/5Ce-FHA and 40Sr/5Ce-FHA has resulted in improved mechanical properties and bioactivity which may accelerate bone formation and could be used for various biomedical applications.

Acknowledgements The authors wish to acknowledge Pondicherry Center for Biological Sciences (PCBS), Puducherry for extending the lab facilities to conduct the cell culture studies. Authors would also like to thank St. Joseph's College, Trichy and Alaggappa University, Karaikudi for the spectral facilities. Authors wish to acknowledge NIT, Trichy for Mechanical studies and Sastra University for SEM studies.

Compliance with ethical standards

Conflict of interest The authors declare that they have no competing interests.

References

1. Dorozhkin SV (2010) Bioceramics of orthocalcium phosphates. Biomaterials 31:1465–1485
2. LeGeros RZ, LeGeros JP (1993) An introduction to bioceramics: dense hydroxyapatite. World Scientific Publishing Co, Singapore
3. Fung YC (1993) Biomechanics: mechanical properties of living tissues. Springer, New York
4. Boanini E, Gazzano M, Bigi A (2010) Ionic substitutions in calcium orthophosphates synthesized at low temperature. Acta Biomater 6:1882–1894
5. Rodrıguez-Lorenzo LM, Hart JN, Gross KA (2003) Influence of fluorine in the synthesis of apatites. Synthesis of solid solutions of hydroxyl-fluorapatite. Biomaterials 24:3777–3785
6. Eslami H, Hashjin MS, Tahriri M (2009) The comparison of powder characteristics and physicochemical, mechanical and biological properties between nanostructure ceramics of hydroxyapatite and fluoridated hydroxyapatite. Mater Sci Eng C 29:1387–1398
7. Bianco A, Cacciotti I, Lombardi M, Montanaro L, Bemporad E, Sebastiani M (2010) F-Substituted hydroxyapatite nanopowders: thermal stability, sintering behavior and mechanical properties. Ceram Int 36:313–322
8. Harrison J, Melville AJ, Forsythe JS, Muddle BC, Trounson AO, Gross KA et al. (2004) Sintered hydroxyfluorapatite-IV: the effect of fluoride substitutions upon colonization of hydroxyapatites by mouse embryonic stem cells. Biomaterials 25:4977–4986
9. Ohno M, Kimoto K, Toyoda T, Kawata K, Arakawa H (2013) Fluoride-treated bio-resorbable synthetic nonceramic [corrected] hydroxyapatite promotes proliferation and differentiation of human osteoblastic MG-63 cells. J Oral Implant 39(2):154–160
10. Uysal I, Severcan F, Tezcaner A, Evis Z (2014) Co-doping of hydroxyapatite with zinc and fluoride improves mechanical and biological properties of hydroxyapatite. Prog Nat Sci 24:340–349
11. Barinov SM, Rustichelli F, Orlovskii VP, Lodini A, Oscarsson S, Fristov SA et al. (2004) Influence of fluorapatite minor additions on behavior of hydroxyapatite ceramics. J Mater Sci Mater Med 15:291–296
12. Chen Y, Miao X (2005) Thermal and chemical stability of fluorohydroxyapatite ceramics with different fluorine contents. Biomaterials 26:1205–1210
13. Wang Y, Zhang S, Zeng X, Ma LL, Wang W, Yan W et al. (2007) Osteoblastic cell response on fluoridated hydroxyapatite coatings. Acta Biomater 3:191–197
14. Qu HB, Wei M (2006) The effect of fluoride contents in fluoridated hydroxyapatite on osteoblast behavior. Acta Biomater 2:113–119
15. Canalis E, Hott M, Deloffre P, Tsouderos Y, Marie PJ (1996) The divalent strontium salt S12911 enhances bone cell replication and bone formation in vitro. Bone 18:517–523
16. Grynpas MD, Hamilton E, Cheung R, Tsouderos Y, Deloffre P, Hott M, Marie PJ (1996) Strontium increases vertebral bone volume in rats at a low dose that does not induce detectable mineralization defect. Bone 18:253–259
17. Marie PJ, Ammann P, Boivin G, Rey C (2001) Mechanisms of action and therapeutic potential of strontium in bone. Calcif Tissue Int 69(3):121–129
18. Zhang W, Shen Y, Pan H, Lin K, Liu X, Darvwell BW et al. (2011) Effects of strontium in modified biomaterials. Acta Biomater 7(2):800–808
19. Webster TJ, Massa Schlueter EA, Smith JL (2004) Osteoblast response to hydroxyapatite doped with divalent and trivalent cations. Biomaterials 22:2111–2121
20. Webster TJ, Ergun C, Domerus RH, Siegel RW, Bizios R (2000) Enhanced functions of osteoblasts on nanophase ceramics. Biomaterials 21:1808–1810
21. Webster TJ (2000) Specific proteins mediate enhanced osteoblast adhesion on nanophase ceramics. J Biomed Mater Res 51:475–483
22. Landi E, Tamperi A, Cellotti G, Spiro S, Sandri M, Logroscino G (2007) Sr-Substituted hydroxyapatite for osteoporotic bone replacement. Acta Biomater 3:961–969
23. Ni GX, Lu WW, Xu B, Chiu KY, Yang C, Li ZY et al. (2006) Interfacial behavior of strontium-containing hydroxyapatite cement with cancellous and cortical bone. Biomaterials 27:5127–5133
24. Blake GM, Fogelman I (2006) Strontium ranelate: a novel treatment for postmenopausal osteoporosis: a review of safety and efficacy. Clin Interv Aging 1:367–375
25. Romieu G, Garric X, Munier S, Vert M, Boudville P (2010) Calcium–strontium mixed phosphate as novel injectable and radio-opaque hydraulic cement. Acta Biomater 6:3208–3215
26. Renaudin G, Laquerriere P, Fillinchuk Y, Jallot E, Nedelec JM (2008) Structural characterization of sol–gel derived Sr-substituted calcium phosphates with anti-osteoporotic and anti-inflammatory properties. J Mater Chem 18:3593–3600
27. Landi E, Sprio S, Sandri M, Celotti G, Tampieri A (2008) Development of Sr and CO3 co-substituted hydroxyapatites for biomedical applications. Acta Biomater 4:656–663
28. Sanyal V, Ramachandra raja C (2016) Synthesis, characterization and in-vitro studies of strontium-zinc co-substituted fluorohydroxyapatite for biomedical applications. J Non-cryst Sol 445–446:81–87. doi:10.1016/j.jnoncrysol.2016.05.010
29. Neilson P (2004) The biological role of strontium. Bone 35 (3):583–588
30. Lin Y, Yang Z, Cheng J (2007) J Rare Earths 25(4):452
31. Gopi D, Ramya S, Rajeswari D, Karthikeyan P, Kavitha L (2014) Strontium, cerium co-substituted hydroxyapatite nanoparticles: synthesis, characterization, antibacterial activity towards prokaryotic strains and in vitro studies. Colloids Surf A 451:172–180
32. Sanyal V, Ramachandra raja C (2016) Structural and antibacterial activity of hydroxyapatite and fluorohydroxyapatite co-substituted with zirconium-cerium ions. Appl Phys A 122(132):1–12. doi:10.1007/s00339-016-9621-x
33. Feng Z, Liao Y, Ye M (2005) Synthesis and structure of cerium substituted hydroxyapatite. J Mater Sci 16:417–421
34. Dal J, Bose S, Bandyopadhyay A (2013) Influence of pentavalent dopant addition to polarization and bioactivity of Hydroxyapatite. Mater Sci Eng C 33(5):3061–3068
35. Kim IS, Kumta PN (2004) Sol–gel synthesis and characterization of nano-structured hydroxyapatite powder. Mater Sci Eng B 111:232–236
36. Dean Mo L, Troczynski T, Tseng WS (2001) Water-based sol–gel synthesis of hydroxyapatite: process development. Biomaterials 22:1721–1730

37. Dean Mo L, Yang Q, Troczynski T, Tseng WS (2002) Structural evolution of sol–gel derived hydroxyapatite. Biomaterials 23:1679–1687
38. Masuda Y, Matubara K, Sakka S (1990) Synthesis of hydroxyapatite from metal alkoxides through sol–gel technique. J Ceram Soc 98:1266–1277
39. ASTM (1984) 'E-384-99': A standard test method for microindentation hardness of materials. ASTM, Philadelphia
40. Slosarczyk A, Bialoskorski J (1998) Hardness and fracture toughness of dense calcium-phosphate-based materials. J Mater Sci 9:103–108
41. Deepachitra R, Chamudeswari M, Santosh Kumar M, Kritiga G, Prabu P, Pandimadevi M, Sastry TP (2013) Osteo mineralization of fibrin-decorated grapheme oxide. Carbon N Y 56:64–76
42. Lima IR, Costa AM, Bastos IN, Granjeiro JM, Soares GA (2006) development and characterization of 5% mol zn bioceramic in granular form. Mater Res 4:399–403
43. Landi E, Tampieri A, Celotti G, Sprio S (2000) Densification behavior and mechanisms of synthetic hydroxyapatites. J Eur Ceram Soc 20:2377–2387
44. Bigi A, Boainini E, Capuccini C, Gazzano M (2007) Strontium substituted hydroxyapatite nanocrystals. Inorg Chim Acta 360 (3):1009–1016
45. Koutopoulos S (2002) Synthesis and characterization of hydroxyapatite crystals: a review study on the analytical methods. J Biomed Mater Res 62:600–612
46. Freund F, Knobel RM (1977) Distribution of fluorine in hydroxyapatite studied by infrared spectroscopy. Dalton Trans J Chem Soc 6:1136–1140
47. Fowler CE, Li M, Mann S, Margolis HC (2005) Influence of surfactant assembly on the formation of calcium phosphate materials—a model for dental enamel formation. J Mater Chem 15:3317–3325
48. Badraoui B, Aissa A, Bigi A, Debbabi M, Gazzano M (2009) Synthesis and characterization of Sr(10-x) Cdx(PO4)6Y2 Y(OH, F): a comparison of apatites containing two divalent ions. Mater Res Bull 44:522–530
49. Bigi A, Gazzano M, Foresti E, Roveri N (1986) Thermal stability of cadmium-calcium hydroxyapatite solid solutions. Dalton Trans J Chem Soc 1:241–244
50. Fowler BO (1974) Infrared studies of apatites. II. Preparation of normal and isotopically substituted calcium, strontium, and barium hydroxyapatites and spectra-structure-composition correlations. Inorg Chem 13:197–214